Ceramics-Silikáty 69 (2), 240-253 (2025)
www.ceramics-silikaty.cz doi: 10.13168/cs.2025.0009

PROPERTIES OF SOLIDIFIED LOESS WITH BASIC MAGNESIUM SULFATE CEMENT

XIAOLONG QI*, #CHENGYOU WU**, ***

*School of Civil Engineering and Water Resources, Qinghai University, Xining 810016, China
**School of Chemical Engineering, Qinghai University, Xining 810016, China
***Qinghai Provincial Key Laboratory of Salt Lake Chemical Engineering Materials

#E-mail: wuchengyou86@163.com

Submitted November 5, 2024, accepted February 18, 2025

Keywords: Loess, basic magnesium sulfate cement (BMSC), unconfined compressive strength, microstructure, unconsolidated undrained triaxial shear test

Typical soil solidifiers, such as ordinary Portland cement, have a limited solidification effect when used as solidifiers, and they can cause significant environmental pollution during the manufacturing phase. Therefore, a relatively green and environmentally friendly solution based on magnesium sulfate cement (BMSC) is explored as a solidifying agent for solidifying the soil. The present paper undergoes a systematic compaction experiment, an unconfined compressive strength test, and an unconsolidated undrained triaxial shear parameters test of BMSC solidified soil with different magnesium oxide (MgO) contents when BMSC was used as the soil stabiliser and the physical properties of BMSC solidified soil were analysed by the techniques of X-ray diffraction (XRD), scanning electron microscopy-energy spectrometry (SEM-EDS), XAn analysis was conducted on the mechanical properties and microstructure of BMSC solidified loess. When the molar ratio is determined, the maximum dry density increases with the increasing magnesium oxide doping. The results indicate that the compressive strength of BMSC solidified loess increases with the increase in the MgO content. Specifically, the compressive strength of the 6 % BMSC solidified loess specimen increased by 528 % compared with that of the pure loess specimen. Moreover, the maximum deviation stress increased by 236.54 %, while the cohesion and internal friction angle increased by 221.89 % and 44.27 %, respectively. The XRD and-ray computed tomography (X-CT), and mercury intrusion porosimetry (MIP). SEM/EDS analyses revealed a great number of 517 ($5Mg(OH)_2$–$MgSO_4$–$7H_2O$) whiskers crisscrossing between the soil particles, which made the microstructure of the BMSC solidified loess specimen denser. The MIP results showed that the macropores and porosity reduction decreased from 43.30 % of the pure loess to 37.01 % in the 6 % BMSC solidified soil specimen. Similarly, the X-CT results revealed a higher pore density and larger porosity in pure loess.

INTRODUCTION

China's loess is primarily distributed in the Loess Plateau region, covering 6.3% of the national territory, while widely distributed, Qinghai Province, located in the western edge of China's main distribution area of wet subsidence loess. The distribution area of loess in Qinghai Province is 24,800 km^2, accounting for 3.9 % of the national loess distribution area, which can be seen in Figure 1, the loess distribution area. Loess is characterised by chalk particles rich in carbonates, having high porosity, water sensitivity and permeability. The property of loess collapsibility refers to the destroyed soil structure under pressure and immersion, which leads to soil subsidence. The tendency of loess to lose strength and soften upon exposure to water poses significant risks to buildings, leading to uneven settlement and foundation subsidence. According to (Zhang et al. (2020a) [1], geohazards, particularly in loess regions, are becoming increasingly frequent in northern China due to more extreme weather events. Data from the Geological Hazard Survey-084 Geological Hazard Survey Report of Loess Region indicate that approximately 30 % of geological disasters occur annually in the Loess Plateau, aside from those triggered by extreme events. Therefore, it is essential to enhance the research and management of geological disaster-prone zones, in the meantime, it is crucial to accelerate the research on curing agents and select those with stable curing effects that are environmentally friendly.

Soil curing is a widely used method for soil improvement in geotechnical engineering, with cement and lime being the most common curing agents in recent years. However, a significant drawback of ordinary Portland cement (OPC) is during the production process, a large amount of CO_2 is generated and a significant amount of energy is consumed, resulting in an increasing environmental burden (Pobłocki et al., 2024) [2]. This makes OPC an environmentally unfriendly binder for loess. Additionally, conventional OPC based agents exhibit limitations in their mechanical strength, durability, and volumetric stability given the essential role of cement in construction and development, thus there is an urgent need to develop environmentally sustainable alternative

cementitious materials. The production of OPC generates between 0.7 to 1.0 tonnes of CO_2 per tonne of cement, while also depleting large quantities of non-renewable resources (N.T. Dung et al., 2017) [3].

Basic magnesium sulfate cement (BMSC) is an environmentally friendly cementitious material known for its lightweight, high strength, excellent abrasion and salt resistances. It is generally used in construction materials, biomaterials, and in other fields. The salt lakes in Qinghai, China, have abundant reserves of high-grade magnesium salt, making it a suitable source for BMSC production. Research indicates that incorporating BMSC as a curing agent into loess leads to the formation of whisker-like ($5Mg(OH)_2$–$MgSO_4$–$7H_2O$) 5-1-7 phases on the surfaces of soil particles and within the pores. This effectively cements soil particles, fills voids, and significantly enhances the mechanical properties of the loess. However, BMSC as a soil curing agent has not yet received sufficient attention, with limited research and experimentation. Further investigation is needed to determine the optimal raw material proportions and curing methods for BMSC, while the properties of BMSC solidified loess and its underlying micro-mechanisms remain to be fully explored. Our group developed a new type of MgO–$MgSO_4$–H_2O cementitious material BMSC by using magnesite, waste sulfuric acid, and industrial waste (slag, fly ash, and magnesium oxide by-products) as the primary raw materials, along with different chemical admixtures. 5-1-7 whiskers, which are the main hydration products of BMSC, have significantly improved mechanical properties compared to Portland cement [4, 5]. We speculate that the energy consumption for producing BMSC is at least 20-30 % lower than that for producing CO_2.

Figure 1. The loess is sourced from Qinghai province.

In this study, the mechanical properties and microstructure of BMSC solidified soil were investigated. The effects of BMSC on the compressive strength and shear strength parameters of the solidified soil were investigated. X-ray diffraction (XRD), scanning electron microscopy (SEM), mercury intrusion porosimetry (MIP), and X-ray computed tomography (X-CT) techniques were employed to analyse the microstructure of the BMSC solidified soil. The specific experimental procedure is illustrated in Figure 2.

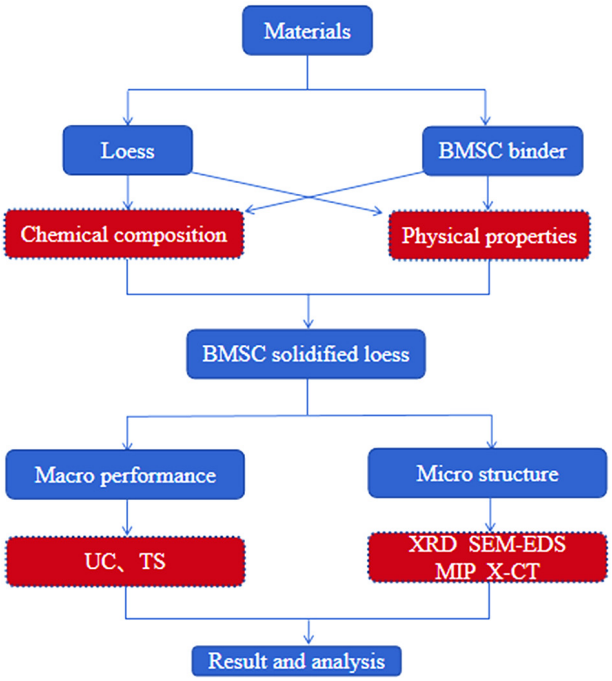

Figure 2. The flow chart of the research approach.

EXPERIMENTAL METHODS AND MATERIALS

Raw materials

The loess selected for the experiment is a fine-grained soil with plasticity index 10.6, whose technical specifications are detailed in Table 1. The BMSC was prepared from light burned magnesite (LBM) and industrial magnesium sulfate. The LBM was produced by calcining magnesite from Liaoning, China, at 1000 °C, resulting in a MgO content of 82.62 % and active MgO content of 55.7 %. The chemical compositions of the loess and the LBM are presented in Table 2. The used industrial magnesium sulfate ($MgSO_4·7H_2O$) was 100 % pure, as was the additive sodium citrate ($C_6H_5Na_3O_3$).

Table 1. Physical indicators of the loess.

Natural density ($g·cm^{-3}$)	Maximum dry density ($g·cm^{-3}$)	Optimum moisture content (%)	Plastic limit (%)	Liquid limit (%)
1.475	1.732	14.32	14.95	25.55

Table 2. Chemical composition (wt. %) of the LBM and loess.

Material	MgO	SiO_2	Al_2O_3	Fe_2O_3	CaO	CO_2	K_2O	Na_2O	P_2O_5	SO_3
Loess	3.55	46.6	13.2	4.12	10.6	17.2	2.58	1.58	0.177	0.144
LBM	85.62	8.94	1.16	1.46	1.18	0	1.64	0	0	0

Sample preparation

In this study, the mixing ratios of all the samples were expressed as molar ratios, with the molar ratio of MgO/$MgSO_4$ (H) was set at 5 and 7. MgO was incorporated at levels of 0 %, 2 %, 3 %, 4 %, and 6 % by mass of the loess. $C_6H_5Na_3O_3$ was added at 0.5 % by the mass of MgO. The optimal moisture content and maximum dry density for the BMSC solidified loess, determined by the compaction test, were 14.67 % and 1.897 g·cm^{-3}. When preparing the solution, $MgSO_4 \cdot 7H_2O$ and $C_6H_5Na_3O_3$ were first mixed with water and thoroughly stirred until fully dissolved. Next, MgO was mixed with the loess and stirred uniformly. The resulting mixture was then slowly stirred for 90 seconds and quickly stirred for an additional 60 seconds in a JJ-5 cement sand mixer, stirring until completed. After mixing, the mixture was covered with plastic wrap for preservation. Cylindrical specimens with a height of 80 mm and a diameter of 39.1 mm were compacted to 95 % of the corresponding dry density using a portable soil compactor. The specimens were then placed in a conservation box at 95 % relative humidity and 20 °C until reaching the required curing age, after which the corresponding experiments were conducted.

Experimental methods

Compressive strength test

The compressive strength of BMSC solidified soil was tested after 3, 7, 14, and 28 days of curing. The tests were conducted using a universal testing machine at a loading rate of 0.3 kN·s^{-1}.

Unconsolidated undrained triaxialshear test

A triaxial shear test was performed on the samples cured for 3, 7, 14, and 28 days. The samples were categorised into five groups based on the MgO content levels (0 %, 2 %, 3 %, 4 %, and 6 %), with each group consisting of three samples. The unconsolidated-undrained (UU) triaxial shear test was conducted using an SLB-1 stress-strain-controlled triaxial shear tester. The designed confining pressures were 50 kPa, 100 kPa, and 150 kPa, with a shear strain rate of 0.8 mm·min^{-1}.

X-ray diffraction test

The BMSC cured soil specimens after reaching the specified age were ground into a powder, and the XRD patterns were collected with an X-ray diffractometer (D/max-2500PC) at an accelerating voltage of 40 kV, with the scanning angle between 5 and 70°, and the scanning speed was kept at 6°·min^{-1}.

Scanning electron microscope

The specimens, after the completion of the maintenance, were dried and sprayed with gold, and the microscopic morphology of the fracture surface of the BMSC cured soil specimens after spraying with gold was observed under a JSM-9700F electron microscope, in which the thickness of the gold spray was 20 nm, and the test voltage was 15 ~ 16 kV and were combined with the EDS spectrometer for the energy spectroscopy analysis.

X-ray microscope test

An Xradia 515 versa 3D X-ray microscope was utilised to obtain three-dimensional images of the samples. This technique was used to analyse and characterise the sample structure in both two and three dimensions and to construct a three-dimensional model of the interior. Scanning was conducted with 1450 projections, each having an exposure time of 6 seconds.

Mercury intrusion porosimetry

For the pore size distribution and porosity analysis, the samples were first cut into small pieces after 28 days of curing and dried at 60 °C for 4 hours. The porosity and pore size distribution of the BMSC solidified loess samples after 28 days of curing were determined using an Auto Pore IV 9500 mercury porosimeter. The pressure range of the instrument was from 1.38 to 228 kPa, the testable pore sizes ranged from 5 nm to 1100 nm, and the contact angle of the mercury with the material was 135 degrees.

RESULTS AND DISCUSSION

Compaction experiment

When the molar ratio is determined, with the increase in the MgO doping, the content of $MgSO_4$ increased. As a soluble sulfate, the increase in the $MgSO_4$ content increases the ion concentration in the soil, the thickness of the diffusion layer becomes thinner. On the one hand, the ability of the soil particles to be bound with water decreases, resulting in a decrease in the optimal moisture content; on the other hand, the resistance between the soil grains decreases, and the soil particles are easy to move and squeeze tightly when compaction is carried out, and the pore space decreases. Then, the maximum dry density increases. The optimum moisture content and maximum dry density of the BMSC solidified loess are presented in Table 3.

Table 3. The optimum moisture content and maximum dry density of the BMSC solidified loess.

	loess	BMSC			
		2 %	3 %	4 %	6 %
Optimum moisture content (%)	14.32	14.96	14.90	14.84	14.67
Maximum dry density ($g \cdot cm^{-3}$)	1.732	1.831	1.854	1.863	1.897

Compressive strength

Figure 3 illustrates the compressive strength of the BMSC solidified soil at several curing ages and MgO dosages. The results indicate that the compressive strength increases progressively with the curing age and is directly proportional to the MgO content. At 28 days, the compressive strength of M6H5 was 2.2 MPa, and the compressive strengths of M4H5, M3H5, M2H5, and M0 were 1.45 MPa, 1.24 MPa, 1.15 MPa, and 0.35 MPa, respectively. This demonstrates that the MgO content significantly improves the compressive strength of the BMSC solidified soil. The compressive strength of M6H7 reached 1.98 MPa at 28 d. The compressive strengths of M4H7, M3H7, and M2H7 were 1.98 MPa, 1.24 MPa, 1.02 MPa, and 0.84 MPa, respectively. Based on the data on the compressive strengths, it can be deduced that the compressive strength increases with the doping amount and age, and that compressive strength of the specimens with H = 7 is smaller than those for H = 5 at all ages. The compressive strength is smaller because the concentration of the $MgSO_4$ solution is reduced and less 5-1-7 phases are generated, so the specimen with H = 7 performs worse in mechanical properties than the specimen with H = 5. Moreover, the enhancement mechanism of H = 5 can be further elucidated through a microstructural analysis.

Triaxial shear test

Stress-strain relationship

By analysing the data of the triaxial shear test on the loess, the stress-strain relationship and the change characteristics of the shear strength of this loess were obtained. The stress-strain curves for the BMSC solidified loess under different MgO content and curing ages at 50 kPa, 100 kPa, and 150 kPa confining pressures are shown in Figure 4. The stress-strain curves of the pure loess specimen exhibit a strain hardening type at the age of 7 days. In contrast, the stress-strain curves of the solidified loess specimens of BMSC exhibit a strain softening type with a significant peak deviation stress at all the confining pressures studied (50 kPa, 100 kPa and 150 kPa). This may be due to the hydration reaction of BMSC, which produces a large amount of hydration products that fill up the pores between the loess particles, so that the soil particles form a connection with each other, increasing the contact surface and contact points between the soil particles, making the occlusion between the loess particles become tighter.

In addition, it can be seen from Figure 4 that the addition of BMSC leads to a significant increase in the ultimate destructive stress of the solidified loess. The peak deviation stress of the solidified soil increased significantly with both the MgO content and the curing age, which shows that the effect of BMSC on the solidified loess is very significant.

It can be also seen from Figure 5 that the stress-strain curves of each cured soil specimen at different molar ratios showed a strain softening type at different ages, and the inflection points appeared on each stress-strain curve. The peak strength of H = 5 was higher than the strength of BMSC cured soil with H = 7. This may be due to the fact that as the molar ratio decreases, the concentration of the $MgSO_4$ solution increases so that

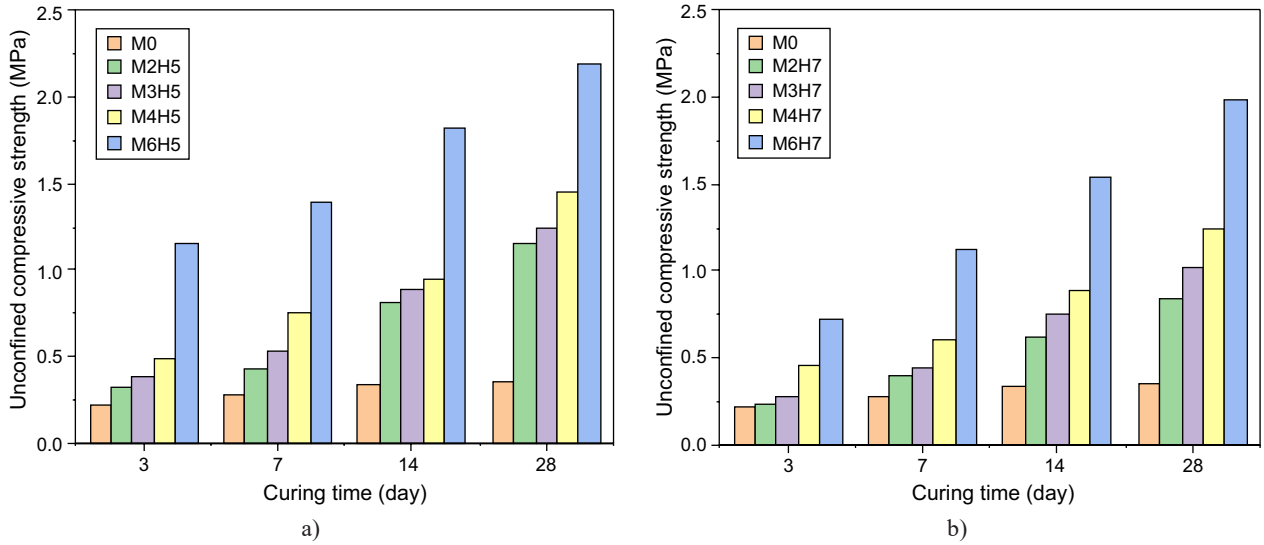

Figure 3. Different MgO content and molar ratios on the un-confined compressive strength of the BMSC solidified loess.

the 5-1-7 phase is produced relatively more, which fills up the pores between the loess particles and wraps the loess particles tightly, so that a connection is formed between the soil particles, which increases the contact surfaces and contacts between the soil particles.

Maximum deviation stress

The peak stress represents the maximum deviation stress, which indicates the peak shear strength. Figure 6 demonstrates that the BMSC significantly increases the maximum deviation stress of the solidified loess compared to the pure loess specimens, the increase is

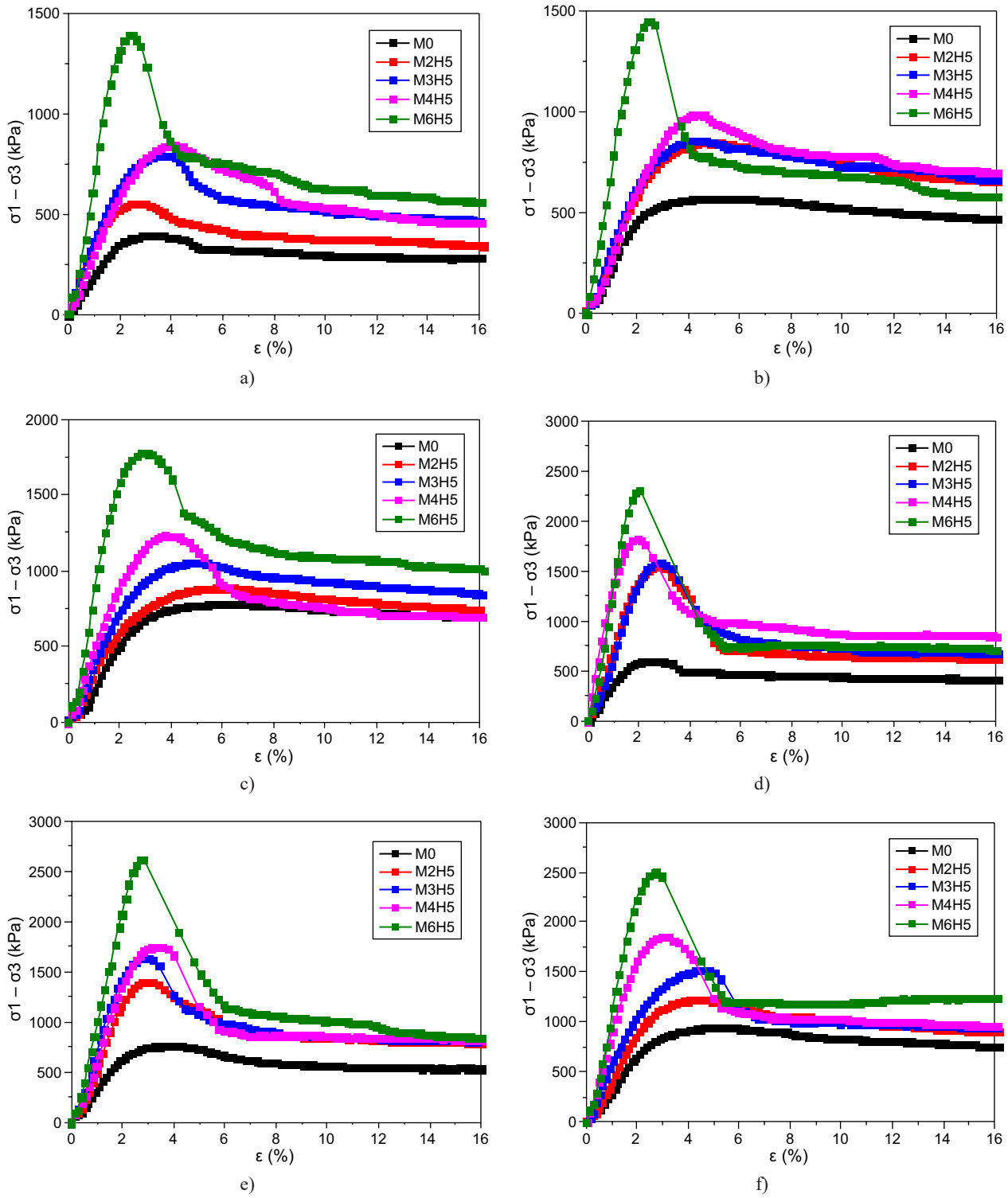

Figure 4. Stress-strain curves of the BMSC solidified loess with different MgO contents under different confining pressures with H = 5: a), b), c) different confining pressures after curing 7 days; d), e), f) different confining pressures after curing 28 days.

attributed to the hydration reaction of the BMSC that produces a large amount of hydration products, which enhances the bonding between the soil particles and increases the bonding between the particles. During the unconsolidated undrained triaxial shear test, the strength of the BMSC solidified loess specimens was significantly higher than that of the pure loess specimens when the mix ratio was M6H5, which indicates that the BMSC reacted most adequately, produced sufficient hydration products, and encapsulated the soil particles tightly.

When the curing age is 3 days and the confining pressure is 50 kPa, the maximum stress increases with the increase in the MgO content, which indicated that the added BMSC reacted at such an early stage and played

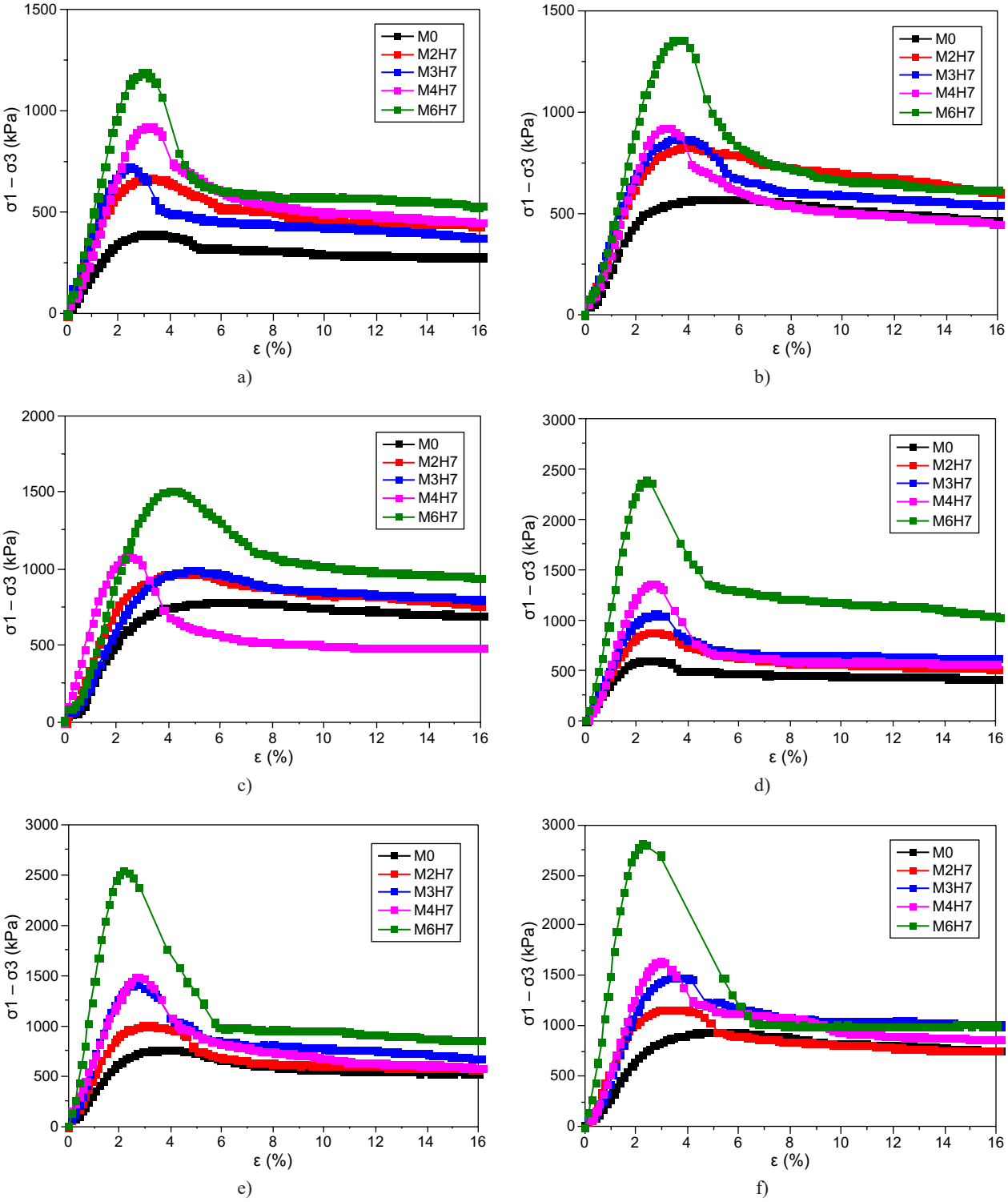

Figure 5. Stress-strain curves of the BMSC solidified loess with different MgO contents under different confining pressures with H = 7: a), b), c) different confining pressures after curing 7 days. d), e), f) different confining pressures after curing 28 days.

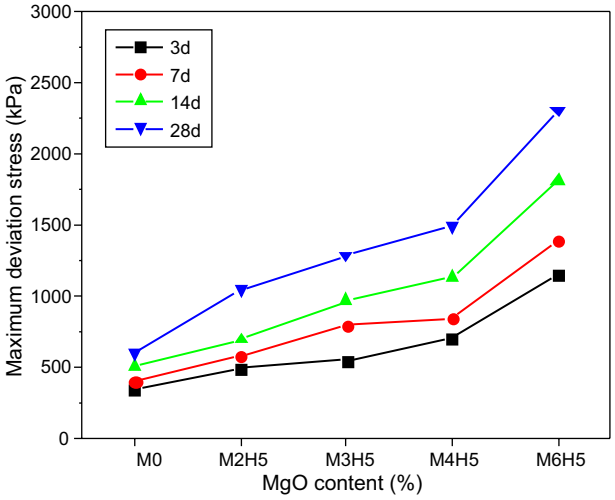

a)

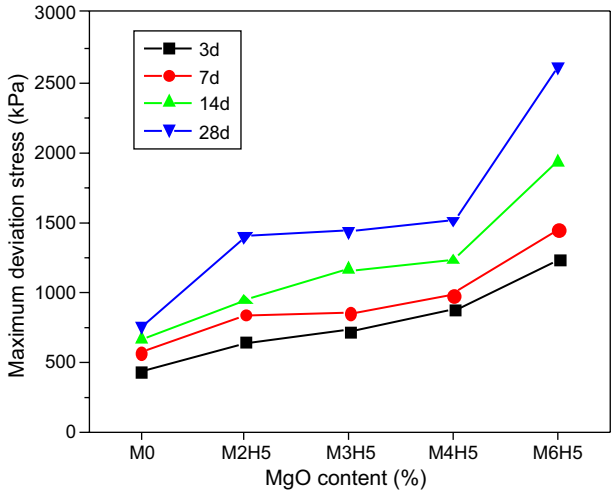

b)

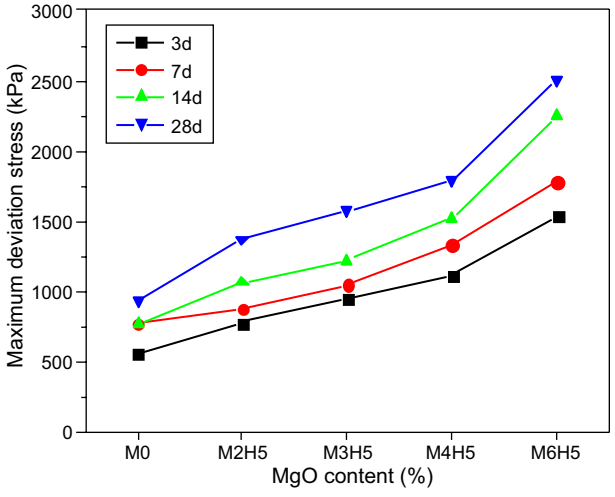

c)

Figure 6. Maximum deviation stress of the BMSC solidified loess with H = 5. The confining pressure is: a) 50 kPa, b) 100 kPa, c) 150 kPa.

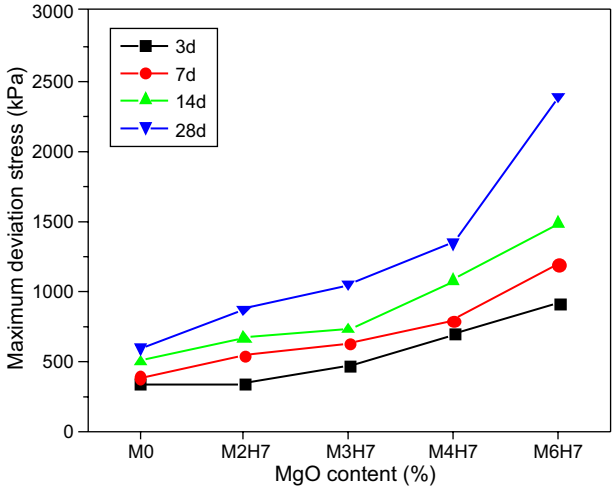

a)

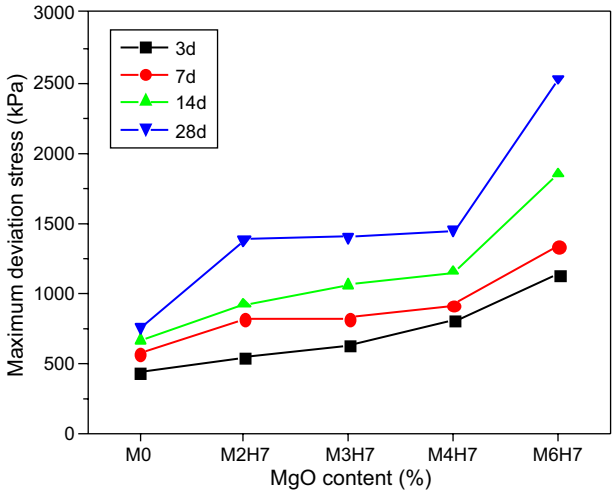

b)

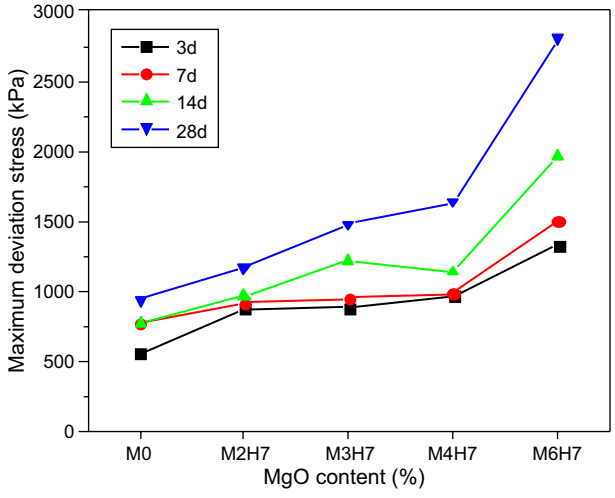

c)

Figure 7. Maximum deviation stress of the BMSC solidified loess with H = 7. The confining pressure is: a) 50 kPa, b) 100 kPa, c) 150 kPa.

a significant role in the solidified soil. The maximum deviation stress continued to rise with the curing age, peaking at 28 days, which can be attributed to the continuous hydration reaction of BMSC.

The shear strength of the solidified loess specimens with the same amount of MgO content gradually increased with the increase in the confining pressure. In this respect, the volume compression of the specimen increases gradually with the increase in the confining pressure. Because the loess particles are close to each other, the interaction force between the soil increases, resulting in an increase in the shear strength of the samples.

It is well known that H = 5 has a higher concentration of the $MgSO_4$ solution than H = 7. The higher the concentration, the more favourable it is for the reaction with MgO, which makes it easier to form the 5-1-7 phase, and more 5-1-7 phases appeared when H = 5 was used. The comparison of Figure 6 and Figure 7 reveals that the maximum deviatoric stresses at the same age for H = 5 is larger than those for H = 7.

Table 4. Inter friction angle and cohesion at the different molar ratios.

Samples	Inter friction angle (°)	Cohesion (kPa)
M0	27.73	111.35
M2H5	34.5	128.59
M3H5	36.052	196.52
M4H5	38.2	230.55
M6H5	40.007	358.42
M0	27.73	111.35
M2H7	29.74	125.49
M3H7	31.578	173.8
M4H7	34.62	193.46
M6H7	38.55	287.62

Shear strength parameters

Table 4 presents the shear strength parameters of the BMSC solidified soil with diverse MgO contents and molar ratios at 28 days, derived from fitting the experimental data with the primary and secondary stresses.

The variation in the Mohr Coulomb shear strength parameters of the solidified loess specimen with the BMSC is shown in Figure 8. The Mohr Coulomb strength parameters (cohesion and angle of internal friction) were determined by the Mohr stress circle obtained when the confining pressures were 50 kPa, 100 kPa, and 150 kPa, respectively. It can be shown from Figure 8 that the cohesion and internal friction angle of the BMSC solidified loess specimens were greatly improved with the increase in the MgO content, and the cohesion and internal friction angle of the BMSC solidified loess specimens were much higher than that of the pure soil, especially when the MgO content was at the maximum of 6 %, the cohesion at 28 d was 358.42 kPa and the internal friction angle was 40.007°, which was higher compared to that of pure loess by 221.89 % and 44.27 %, respectively.

Changes in the cohesion are usually indicative of the degree of the BMSC reaction, while changes in the internal friction angle are more likely to indicate changes in the particle rearrangement (slip and interlocking). The cohesion and internal friction angle of the BMSC solidified loess gradually increased with the curing age. The main reason may be the hydration of the BMSC reacting with the soil particles. The newly formed cementitious material filled the pores between the soil particles, changed the arrangement and contact mode of the original soil particles, and transformed the point-point contact into a surface-face contact, thus reducing the pores between the soil particles. This change and the generation of hydration products caused the particles to be more tightly bound.

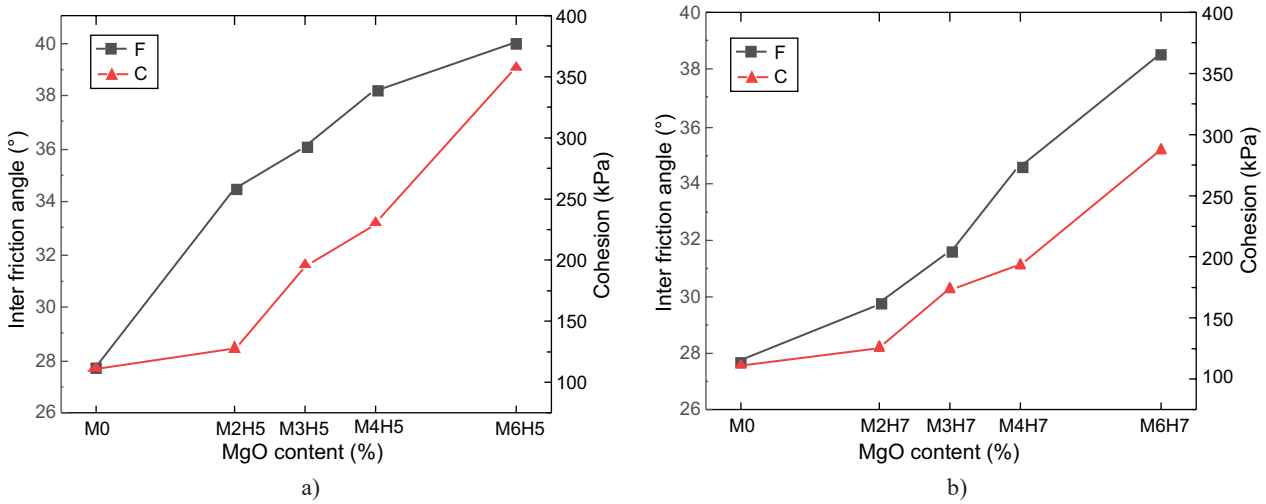

Figure 8. Variation of the Mohr Coulomb shear strength parameter: a) H = 5 internal friction angle and cohesion; b) H = 7 internal friction angle and cohesion.

The specimens with H = 7 reflect the same pattern as those with H = 5, the cohesion and the angle of internal friction increase with the increase in the MgO doping, the specimens with H = 7 will be smaller than the specimens with H = 5, due to the decrease in the concentration of $MgSO_4$, which results in the synthesised 5-1-7 phase being reduced.

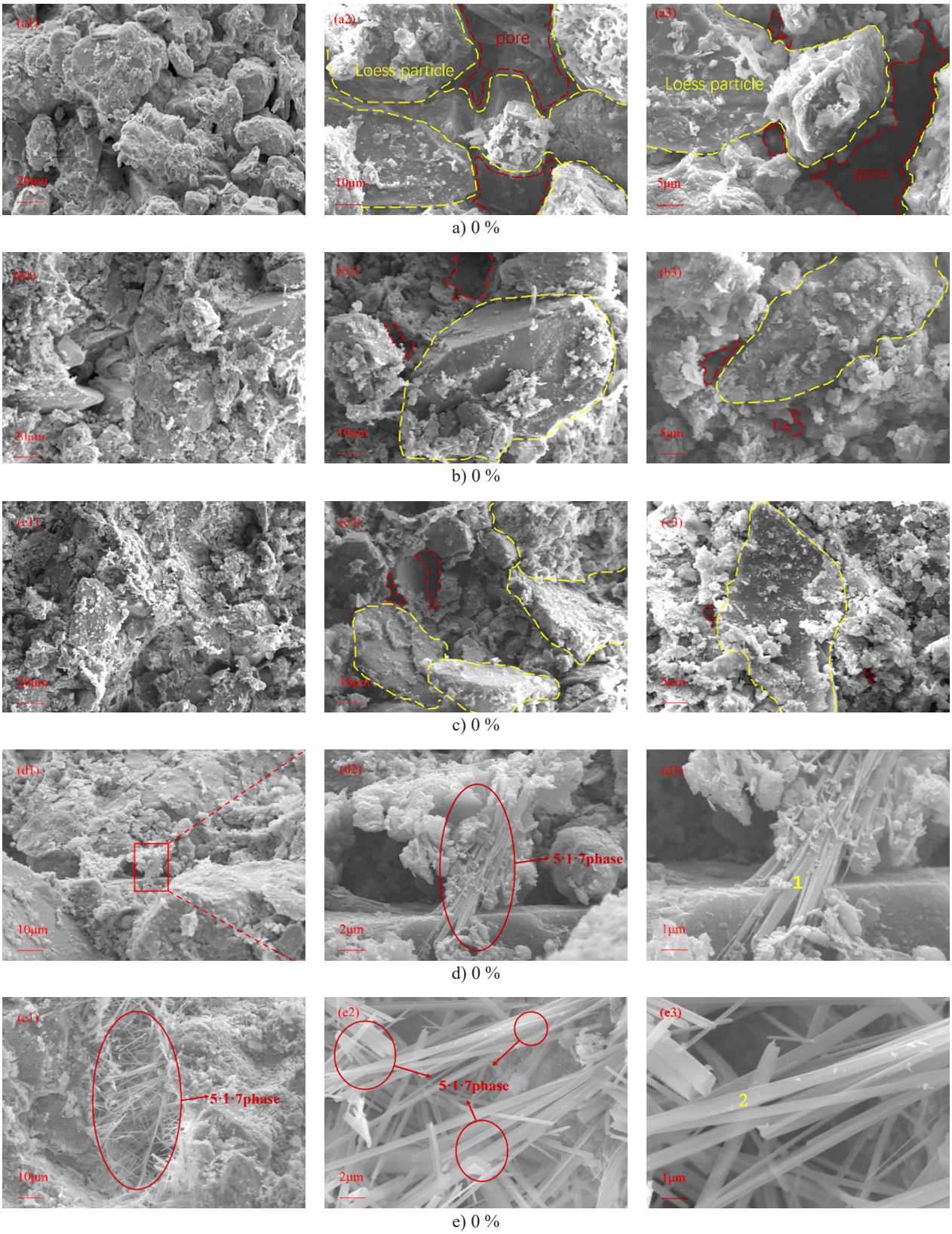

Figure 9. SEM micrographs of the solidified loess samples with different MgO binders. *(Continue on next page)*

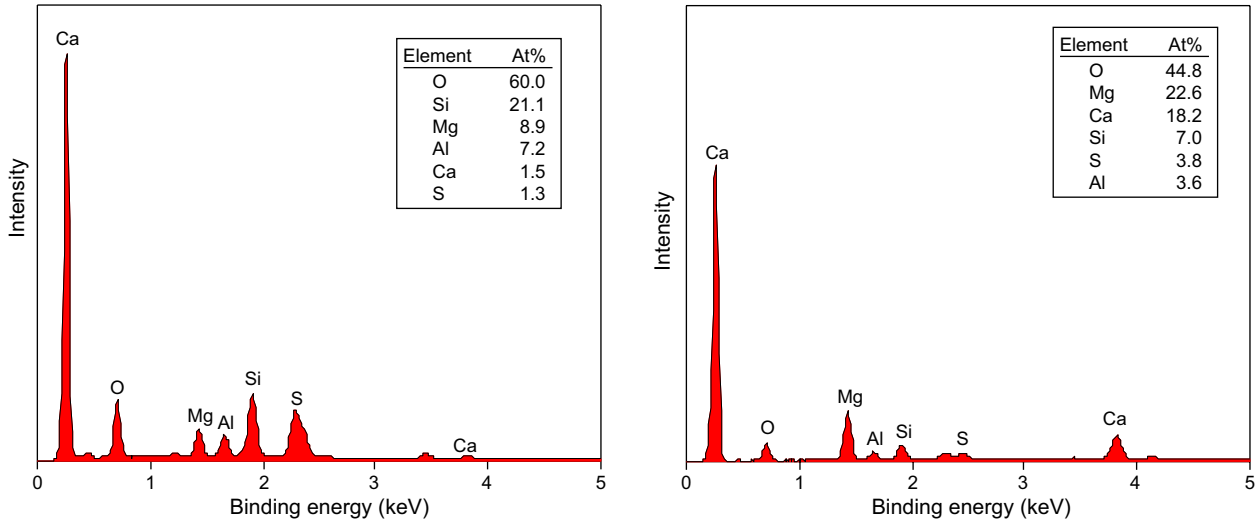

Figure 9. EDS micrographs of the solidified loess samples with different MgO binders.

SEM analysis

Figure 9 presents the microstructure of the BMSC solidified loess with the different MgO content after 28 days of curing. From the SEM images, it can be seen that numerous pores are present in the pure loess. The soil particles exist in the form of granular, flaky and polygonal structures. The soil particles are distinct, and there is a lack of cementitious material between them. After adding BMSC to the soil, the flocculating material becomes visible between the soil particles, the angularity of some soil particles decreases or disappears, and the granular structure diminishes, and the complete soil particles can hardly be seen. The cementitious material and a large number of 5-1-7 whiskers are observed between the particles, significantly reducing the large pores and pore areas. The contact patterns between the particles also changed, most of which were face-to-face contact patterns. The hydration product 5-1-7 whiskers produced by the BMSC filled the pore spaces and exhibited binding properties, weakening the apparent granulation characteristics and enhancing the soil particle integrity.

With the increase in the MgO content, the BMSC produced more and more hydration products, leading to increased particle contact and larger particle size in the solidified loess. Thus, it improved the mechanical properties of the solidified loess. The 5-1-7 whiskers of the M6H5 specimens are the densest, and the soil particles are almost entirely integrated by whiskers as well as gel-like products, therefore the intact soil particles are almost invisible and pores are rarely observed. The differences in the microstructure of the solidified loess were consistent with the changes in the mechanical properties, the denser the microstructure of the solidified loess, the higher maximum deviation stress.

In addition to some lamellar crystals, a large number of needle-and-rod crystals appeared, which were similar to the whiskers with lengths of 10-20 μm, diameters of 0.2-0.5 μm, and length-to-diameter ratios between 20 and 100. Combined with the compound phase composition, it was judged that the needle-rod crystals should be the 5-1-7 phase, which was similar to the 5-1-8 phase in magnesium oxychloride cement, and the needle-rod 5-1-7 phases were intertwined with each other, which made the structure of the solidified loess of the BMSC dense with high strength. A large number of whisker-like crystals can be seen in the BMSC solidified loess specimens at 4% and 6% MgO content, and combined with the EDS results (Figure 9f,g), it can be seen that the molar ratios of Mg/S are about 6.8 and 5.9, which are close to the theoretical ratio of 6.0 for the 5-1-7 phase, thus, the whisker-like hydration product is the 5-1-7 phase.

XRD analysis

The crystal structure changes in the mineral composition of the BMSC solidified loess with different MgO contents were determined by an X-ray diffractometer. From Figure 10, it can be seen that there are some obvious differences in the mineral composition between the pure loess and the BMSC cured soil. After adding the BMSC curing agent, the diffraction peaks of the 5-1-7 phase can be observed, with the increase in the MgO content, the 5-1-7 crystalline phase gradually increases, which indicates that higher amounts of 5-1-7 phases are generated in the BMSC solidified loess specimens. The mineral compositions of the BMSC solidified loess are still dominated by the non-clay minerals of quartz, mica, and limestone.

In the BMSC solidified loess specimens, the higher the 5-1-7 phase content, the higher the strength, M6H5 has been completely hydrated after 28 d of maintenance of MgO, and there is no generation of magnesium hydroxide, MgO reacted with the liquid phase to generate the 5-1-7 phase, and thus the 28-d strength of the M6H5 specimen is the highest.

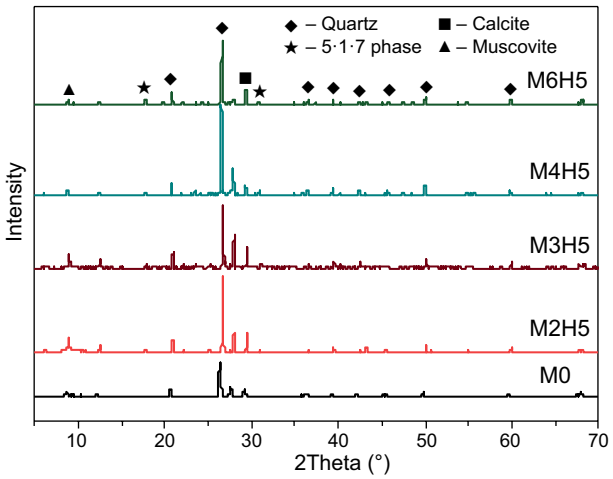

Figure 10. XRD patterns of the BMSC solidified loess.

MIP analysis

Figure 11 shows the cumulative porosity distribution curves of the BMSC solidified loess measured by mercury intrusion porosimetry (MIP) analysis. It can be revealed from these five curves that the porosity decreases with the addition of the BMSC curing agent. Table 5 shows the porosity data obtained from the MIP tests and the results show that with the addition of the BMSC curing agent, the porosity of the soil was 43.30 %, whereas the porosity of M2H5 was 39.91 %, M3H5 was 38.91 %, M4H5 was 38 %, M6H5 was 37.01 %, which were reduced by 7.8 %, 10.1 %, 12.2 % and 14.5 %, respectively. The average pore size of soil was 261.94 nm, while the average pore size of M2H5 was 248.05 nm, M3H5 was 215.86 nm, M4H5 was 179.63 nm, and M6H5 was 154.46 nm, which were 5.3 %, 17.6 %, 31.4 %, and 41 % lower, respectively. It can be concluded that micropores became the major pore type after the addition of the BMSC curing agent. Therefore, the results of the MIP test indicate that the addition of the BMSC curing agent effectively filled the small pores during the compaction process, thus effectively improving the strength of the soil.

Table 5. Statistics of the pore distribution of the BMSC solidified loess curing 28 days.

Samples	Average pore diameter (nm)	Porosity (%)	≤ 100 nm (%)	≥ 100 nm (%)
M0	261.94	43.3077	14.50	85.50
M2H5	248.05	39.9100	34.31	65.69
M3H5	215.86	38.9095	38.15	61.85
M4H5	179.63	38.0009	46.30	53.70
M6H5	154.46	37.0129	58.89	41.11

X-CT analysis

From Figure 12, we can see that the blue areas represent smaller porosity, the green colour represents medium porosity, and the red areas represent large porosity. In the pure loess specimen, we can see that there are a lot of blue areas, and the blue areas are very widely distributed, which also represents its larger porosity, and we can also see the green and red areas, which also indicates that there are a lot of large pores in the pure loess specimen, which indirectly indicates that its mechanical properties are relatively low; after the addition of BMSC, it is still mainly dominated by the micropores in the blue areas, while, compared to the pure

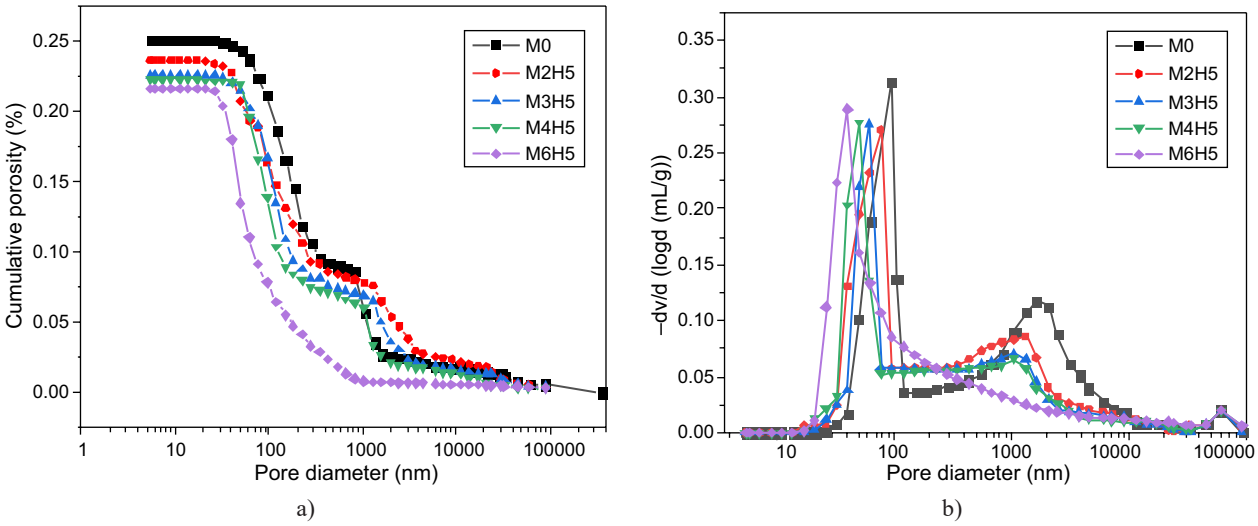

Figure 11. Cumulative porosity (a) and pore size distribution (b) of the BMSC solidified loess.

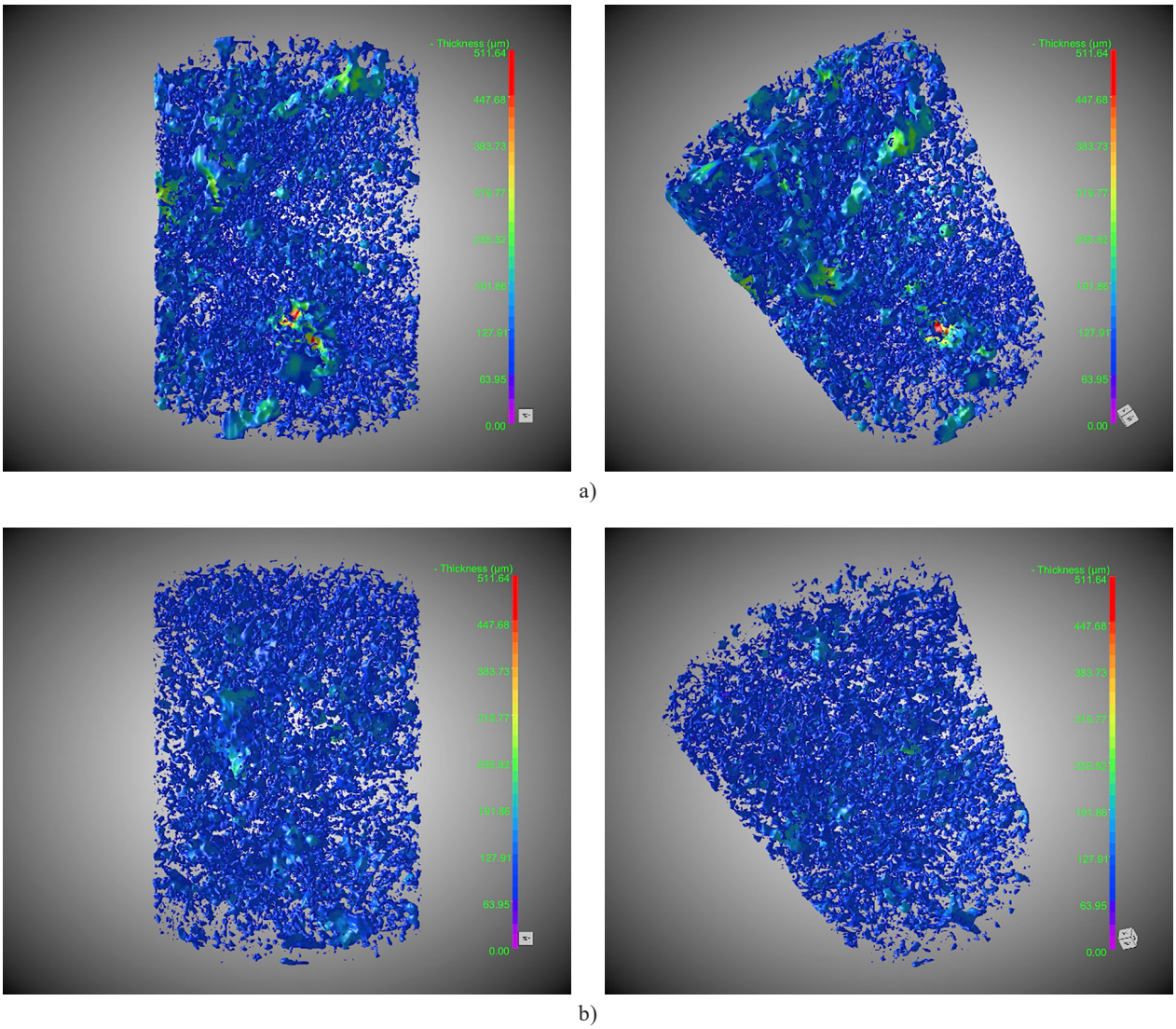

a)

b)

Figure 12. X-CT images of the loess (a) and the 6 % BMSC solidified loess (b).

loess specimen, its distribution density is smaller than that of the latter and some sporadic green areas can also be seen. In general, the BMSC can effectively improve the porosity of the loess and improve the mechanical properties of the loess.

CONCLUSION

In this study, a new type of cementitious material, BMSC, was used to carry out solidified loess experiments. As a curing agent, it has a better solidifying effect and effectively connects the soil particles through the hydration product 5-1-7, and this important discovery highlights its broad prospects in the field of solidified loess:

- When the molar ratio is determined, the optimum moisture content decreases and the maximum dry density increases with the increasing magnesium oxide doping. The mechanical properties of the loess were significantly improved after the incorporation of BMSC with 6 % MgO into the loess, with the most obvious increase in the early compressive strength, which was mainly attributed to the formation of the 5-1-7 phase between the soil particles, and the 5-1-7 phase is the strength phase in magnesium cement, which provided strength support for the solidified loess by BMSC.
- The XRD analysis showed that the introduction of BMSC led to the formation of 5-1-7 phases. The MIP results showed that the reduction of macropores and the porosity of BMSC solidified loess decreased from 43.30 % in the pure soil to 37.01 % in the 6 % BMSC solidified loess, and the average pore size of 261.94 nm decreased to 154.46 nm. The SEM analysis showed that a large amount of 5-1-7 phase formed between the soil particles, which filled the pores and connected the soil particles. The X-CT results indicated that the addition of BMSC to the soil reduced the pores and the density of pore distribution, so the porosity was low.

Acknowledgements

This research was supported by the Natural Science Foundations of Qinghai Province of China [grant number 2023-ZJ-914M] and the National Natural Science Foundations of China [grant number 52462204].

REFERENCES

1. Zhang L., Huang J., Liang J., Yu H., Guan X., Ma J, et al., (2020): Impact of climate change on the Yellow River basin and respons. *Science & Technology Review, 38*(17), 42-51. doi: 10.3981/j.issn.1000-7857.2020.17.004
2. Pobłocki K., Pawlak M., Drzeżdżon J., Gawdzik B., Jacewicz D. (2024): Clean production of geopolymers as an opportunity for sustainable development of the construction industry. *Science of The Total Environment*, 172579. doi: 10.1016/j.scitotenv.2024.172579
3. Dung N. T., Unluer C. (2017): Carbonated MgO concrete with improved performance: The influence of temperature and hydration agent on hydration, carbonation and strength gain. *Cement and Concrete Composites*, *82*, 152-164.doi: 10.1016/j.cemconcomp.2017.06.006
4. Guo T., Wang H., Yang H., Cai X., Ma Q., Yang S. (2017): The mechanical properties of magnesium oxysulfate cement enhanced with 517 phase magnesium oxysulfate whiskers. *Construction and Building Materials*, *150*, 844-850. doi: 10.1016/j.conbuildmat.2017.06.024
5. Zeng X., Yu H. (2018): Experimental study on reinforced concrete large-eccentricity compressive column of basic magnesium sulfate cement concrete – in different curing conditions. *Structural Concrete*, *19*(6), 1608-1618. doi: 10.1002/suco.201700121
6. Chang X., Wang X., Zhai W. (2023): Influence of biopolymer-chitosan on the solidification performance of silt. *Yangtze River, 54,* 211-215.
7. Chen R., Zhang X., Zhu Y. (2023): Steel slag and cement based geopolymer solidification of wetand soft loess: mechanical properties and micro mechanisms. *Journal of Chongqing Jiaotong University (Natural Science), 42*, 55-61.
8. Cheng X., Qi L., Zha W., Zhou Y., Gao F., Zou W. (2022) : Experimental study on cement improved loess. *International Journal of Pavement Research and Technology*, *15*(2), 384-394. doi: 10.1007/s42947-021-00028-y
9. Ding Y., Yang W. (2023): Study on new composite curing agent for improving collapsible loess. *Contemporary Chemical Industry, 52*, 1068-1071+1098.
10. Dong C., Huang Y., Zhang W., Tang X., Gu Y., Feng Y. (2023): Behavioral evaluation on the engineering properties of lignin-stabilized loess: Reuse of renewable materials. *Construction and Building Materials*, *369*, 130599. doi: 10.1016/j.conbuildmat.2023.130599
11. Ghadakpour M., Choobbasti A. J., Kutanaei S. S. (2020): Experimental study of impact of cement treatment on the shear behavior of loess and clay. *Arabian Journal of Geosciences*, *13*, 1-11. doi: 10.1007/s12517-020-5181-7
12. Group, CMIA (2016). *Magnesium cementitious materials and products technology.* China Building Materials Industry Press (in Chinese)
13. He Z., Fan H., Wang J., Liu G., Wang Z., Yu J. (2017): Experimental study of engineering properties of loess reinforced by lignosulfonate. *Rock and Soil Mechanics*, *38*(3), 731-739.
14. Hou C., Ni W., Du H., Liu W. (2020): Effect of admixture on mechanical properties of magnesium oxysulfide cement and analysis of hydration mechanism. *New Building Materials/Xinxing Jianzhu Cailiao*, *47*(4), 1. (in Chinese)
15. Jia Z., Yan C., Li B., Bao H., Lan H., et al. (2023): Performance test and effect evaluation of guar gum-stabilized loess as a sustainable slope protection material. *Journal of Cleaner Production*, *408*, 137085. doi: 10.1016/j.jclepro.2023.137085
16. Jiang Y., Yi Y., Tian T., Sha H., Fan J., Ji X., Xue J. (2022): Water infiltration and water stability of compacted loess roadbeds based on vibration compaction. *Arabian Journal for Science and Engineering*, 1-15. doi: 10.1007/s13369-021-06346-4
17. Lei X. (1987): Pore Types and wetness of Loess in China. *Scientia Sinica (Chimica)*, *12*, 1309-1318.
18. Li C. Q., Liu Q. B., Xiang W., Wang J. E., Qiao Y. (2018): Anti-erodibility of loess subgrade slope reinforced with SH-polymer and inorganic material. *Journal of Changjiang River Scientific Research Institute*, *35*(8), 90-94+101. doi: 10.11988/ckyyb.20170221
19. Li H., Yang M., Guo X. (2023): Study of the disintegration of loess modified with fly ash and Roadyes. *Scientific Reports*, *13*(1), 7253.doi: 10.1038/s41598-023-33434-2
20. Li W., Li L., Deng Z., Wang H., Li W., Kong Y. (2024): Research on the solidification effect of new curing agents on collapsible loess. *Architecture Technology, 55*, 349-353.
21. Li Z. H. (2015). *Reaction Mechanisms and Application Study of MgO–SiO_2–H_2O Cementitious System.* South China University of Technology: Guangzhou, China. (in Chinese)
22. Lin G., Liu W., Zhao J., Fu P. (2023): Experimental investigation into effects of lignin on sandy loess. *Soils and Foundations*, *63*(5), 101359.doi: 10.1016/j.sandf.2023.101359
23. Liu J. (2016): Research on comparison of curing agents of cement and lime fly-ash in loess improvement. *Northern Communications, 6,* 113-116. (in Chinese)
24. Liu J., Luo H., Lei H., Zhang G., Cheng X. (2023): Study on the compressive strength and curing mechanism of alkali-activated geopolymer curing marine silty soft soil. *Journal of Railway Science and Engineering,1,* 1-11. (in Chinese)
25. Liu X., Pan C., Yu J., Fan J. (2021): Study on micro-characteristics of microbe-induced calcium carbonate solidified loess. *Crystals*, *11*(12), 1492.doi: 10.3390/cryst11121492
[26. Runčevski T., Wu C., Yu H., Yang B., Dinnebier R. E. (2013): Structural characterization of a new magnesium oxysulfate hydrate cement phase and its surface reactions with atmospheric carbon dioxide. *Journal of the American Ceramic Society*, *96*(11), 3609-3616. doi: 10.1111/jace.12556
27. Zhang C. L., Jiang G. L., Su L. J., Zhou G. D. (2017): Effect of cement on the stabilization of loess. *Journal of Mountain Science*, *14*(11), 2325-2336.doi: 10.1007/s11629-017-4365-4
28. Zhang Q., Yan N., Wang Y., Qiao F., Bai X. (2024): Development and application of HR soft soil curing agent. *Geotech. Invest. Survey, 1*, 1-5. (in Chinese)
29. Wang X. (2018). Applications of basic magnesium sulfate cement in civil engineering. *Chemical Engineering Transactions*, *66*, 1189-1194. doi: 10.3303/CET1866199
30. Xu X., Xu Y., Duan L. (2018). Effect of fineness and components of CFBC ash on performance of basic magnesium sulfate cement. *Construction and Building Materials*, *170*, 801-811.doi: 10.1016/j.conbuildmat.2018.03.054

31. Hao Y. Z., Wang T. H., Wang Z., Jin X. (2021). Experimental study on triaxial shear characteristics of compacted loess under drying and wetting cycles. *Journal of Hydraulic Engineering*, *52*(3), 359-369.
32. Chau C. K., Li Z. (2008): Accelerated reactivity assessment of light burnt magnesium oxide. *Journal of the American Ceramic Society*, *91*(5), 1640-1645.doi: 10.1111/j.1551-2916.2008.02330.x
33. GB/T 50123-2019 (2019). Standard for Geotechnical Testing Method; Ministry of Housing and Urban-Rural Development of the People's Republic of China: Beijing, China